Cacace, M., Scheck-Wenderoth, M. (2016): Why intracontinental basins subside longer: 3-D feedback effects of lithospheric cooling and sedimentation on the flexural strength of the lithosphere. - *Journal of Geophysical Research*, *121*, 5, pp. 3742—3761.

DOI: http://doi.org/10.1002/2015JB012682

AGU PUBLICATIONS

JGR

Journal of Geophysical Research: Solid Earth

RESEARCH ARTICLE
10.1002/2015JB012682

Key Points:
- Unravel first-order aspect of intracontinental basin evolution
- Highlight the limitations of 1-D/2-D approaches

Supporting Information:
- Supporting Information S1

Correspondence to:
M. Cacace,
mauro.cacace@gfz-potsdam.de

Citation:
Cacace, M., and M. Scheck-Wenderoth (2016), Why intracontinental basins subside longer: 3-D feedback effects of lithospheric cooling and sedimentation on the flexural strength of the lithosphere, *J. Geophys. Res. Solid Earth*, *121*, 3742–3761, doi:10.1002/2015JB012682.

Received 24 NOV 2015
Accepted 18 APR 2016
Accepted article online 20 APR 2016
Published online 3 MAY 2016

Why intracontinental basins subside longer: 3-D feedback effects of lithospheric cooling and sedimentation on the flexural strength of the lithosphere

M. Cacace[1] and M. Scheck-Wenderoth[1,2]

[1]German Research Centre for Geosciences (GFZ), Potsdam, Germany, [2]Department of Geology, Geochemistry of Petroleum and Coal, RWTH Aachen University, Aachen, Germany

Abstract The aim of this study is to reevaluate the character and evolution of the large-scale subsidence of intracontinental basins using 3-D thermomechanical numerical simulations accounting for the coupling between sedimentation, rheology-dependent lithospheric flexure, and thermal contraction by lithospheric cooling. The flexural rigidity of the lithospheric plate is controlled by elastic-brittle-plastic rheology, enabling the computation of thermal and mechanical feedback processes occurring during basin subsidence. Numerical results show that depending on the sediment loading history, a rheological stratified lithosphere can subside over geological time scales without imposition of ad hoc geometric and kinematic initial conditions. Three-dimensional feedback effects of sedimentation on the thermomechanical structure of the plate result in a weakened lower crust mechanically decoupled from the underlying mantle and therefore easily reactivated even under low background stresses. Our results explain the first-order characteristics of the subsidence in intracontinental basins and reconcile basic observations of their deformation history.

1. Introduction

Intracontinental basins are large (up to 1000 km in length), bowl-shaped depressions of the Earth's crust. They formed on stable continental lithosphere far away from active tectonic boundaries during periods of supercontinental breakup. These basins are characterized by a layer cake infill architecture usually associated with a negative free-air gravity anomaly [*Klein and Hsui*, 1987]. Sediment accumulation rates in these settings are extremely slow (from few meters up to 20 m/Myr), and their stratigraphy is predominately terrestrial to shallow marine, indicating a sedimentation that kept pace with their subsidence throughout their history. Given their high preservation potential, intracontinental basins have long been regarded as important archives not only regarding our understanding of the past geodynamic history of the Earth but also in terms of economic aspects [*Lambeck*, 1983; *Littke et al*., 2008; *Sloss*, 1988]. However, they still remain poorly understood from a geodynamic point of view.

The most enigmatic feature of intracontinental basins is a rather uniform, slow, and long-lasting (measured in hundreds of million years) subsidence. Reconstructed tectonic subsidence curves display a sublinear to gently exponential shape, similar to those of passive margins and rifts [*Xie and Heller*, 2009]. However, subsidence in these basins generally lacks a well-developed initial and rapid, rift-like stage as demonstrated by the absence of faulting across their basements [*Xie and Heller*, 2009]. To explain the origin and evolution of intracontinental basins, by reconciling the basic features of their subsidence history, a number of mechanisms have been invoked. A nonexhaustive list comprises the following: density changes within the lower crust and lithospheric mantle due to mineral phase changes [*Gac et al*., 2012; *Kaus et al*., 2005], thermal relaxation and subsidence due to (negative) dynamic topography related to mantle convective instabilities [*Burgess and Gurnis*, 1995; *Burgess et al*., 1997; *Heine et al*., 2012], relaxation of a thick lithosphere under finite strain rates [*Armitage and Allen*, 2010; *Holt et al*., 2010], in-plane stresses and tectonic rejuvenation [*Braun and Shaw*, 2001], and uplift followed by subaerial erosion [*Burov and Cloetingh*, 1997]. Apart from providing a significant advance in our understanding of the continental rifting dynamics, these studies have been able to explain some details of the subsidence history in specific intracontinental settings. However, no model so far has been able to reconcile observations on a more global scale.

Models that require mineral phase changes as preferential mechanisms [*Gac et al*., 2012; *Kaus et al*., 2005] cannot be easily extended to generic intracontinental settings. Variations in the crustal density configuration typically associated to phase changes due to extensional tectonics (e.g., garnet-lhertzolite phase transition) would require (too) high amounts of stretching to have any sensible effect on the subsidence evolution.

However, intracontinental basins lack any sign of extensive deformation by crustal stretching in the form of basement faulting and graben and/or half-graben formation [*Hartley and Allen*, 1994; *Klein and Hsui*, 1987]. An alternative is to assume lower crustal metamorphism as an explanation of the subsidence of intracontinental basins [*Baird et al*., 1995; *Hamdami et al*., 1994]. Lower crust phase transition to denser eclogites might provide enough gravitational load on the lithosphere to affect its subsidence without requiring extensive extensional forces. However, to apply this hypothesis to intracontinental basins requires finding a thermal mechanism causing upwelling of warmer materials at the base of the crust without leaving any surface expressions of the resulting subcrustal load, an aspect for which there is no clear observational evidence [*Klein and Hsui*, 1987; *Lambeck*, 1983; *Pawlak et al*., 2011]. A further drawback of these models is that they must rely on an additional, primary mechanism promoting phase changes and subsidence. However, many intracontinental basins do not show any temporal correlation between the bulk of volcanic activity and their main phases of subsidence.

Viscous flow in the mantle has been demonstrated to be a viable mechanism explaining the basic characteristics of the oceanic lithosphere [*Huang and Zhong*, 2005] and, more recently, the overall stratigraphic patterns observed in rift systems [*Petersen et al*., 2010]. Mantle flow associated to a subducting slab and/or a mantle plume might induce subsidence/uplift in the lithosphere [*Gurnis*, 1988; *Zhong et al*., 1996], but its role in the subsidence of basins within the continental interiors is elusive [*Buiter et al*., 2012; *Kabongo et al*., 2011]. Different studies have demonstrated the relevance of dynamic topography for the stratigraphy of intracontinental basins, such as its influential role in the formation of (mega)sequences and their bounding unconformities [*Burgess and Gurnis*, 1995; *Burgess et al*., 1997; *Coackley and Gurnis*, 1995]. However, the large spatial and long temporal scales of the subsidence of intracontinental basin prove difficult to be accounted for by dynamic topography alone. The long-term preservation potential of these basins cannot be easily reconciled with the time scale typical of mantle flow processes [*Burgess et al*., 1997; *Heine et al*., 2012]. Once the downwelling ceases, the isostatic rebound will lead to uplift followed by erosion of the younger strata, a feature not commonly observed in intracontinental basins. Additionally, as demonstrated by some more recent studies [*Buiter et al*., 2012], the induced deformation might be smaller in magnitude than previously estimated. These aspects indicate that mantle dynamics probably play a secondary role in the subsidence history of intracontinental basins and that other mechanisms must operate to generate their long-term, background subsidence [*Burgess and Gurnis*, 1995].

To reconcile these aspects, an initial extensional stage, possibly associated to continental stretching, followed by a thermal contraction with a longer decay constant is often assumed [*Kaminski and Jaupart*, 2000; *Sleep and Sloss*, 1980]. Uniform stretching models [*McKenzie*, 1978] and minor variants thereof, while able to explain some basic aspects of the basin-forming kinematics, fail to account for the evolution of their subsidence history. Analytical solutions to the plate-cooling models, even when accounting for configurations appropriate for the continental lithosphere [*Armitage and Allen*, 2010], can reconcile observations only for a finite range of steady state plate thicknesses larger than 200 km. While some of the basins in the continental interiors developed on old (Precambrian), thick, and thermally mature continental lithosphere (e.g., Congo, Illinois, and East Barents Sea basins), others overlie a much younger (Phanerozoic) continental lithosphere mainly consisting of young, welded arcs and orogenic belts (e.g., Northeast German, Paris, and Chad basins); see Figure 1. An additional drawback of such one-dimensional models is that they fail to account for both the mechanical feedback effect of lateral differential loading as well as the effects of 3-D heat transfer and related thermal stresses on the strength of the lithosphere. Therefore, they generally overestimate the amount of initial deformation to match observed subsidence curves [*Zhang*, 1993]. These models predict stretching factors high enough to cause extensional brittle deformation in the basement or to initiate decompressional melting in the mantle, features that are not commonly observed in intracontinental settings [*Hartley and Allen*, 1994].

The aim of this study is to reevaluate the long-term character of the subsidence history in intracontinental basins. The goal is to propose viable mechanisms to explain the first-order character of their subsidence by accounting for and reconciling the basic observations done in these settings. In our attempt to address these primary mechanisms, we focus on two major features, which are shared by intracontinental basins worldwide. (1) The basin fill shows only moderate signs of brittle deformation by faulting, the latter being associated with minor thermal disturbances of the lithosphere [*Hartley and Allen*, 1994], and (2) intracontinental basins contain a variably thick sedimentary cover consisting predominately of shallow water and terrestrial sediments. The role of sediments in shaping the thermal and mechanical structure of basins has long been recognized [*Karner*, 1991; *Lavier and Steckler*, 1997], but their effects on the resulting 3-D basin evolution is yet to be properly quantified. The majority of previous studies relied mainly on two-dimensional approximations of the lithosphere

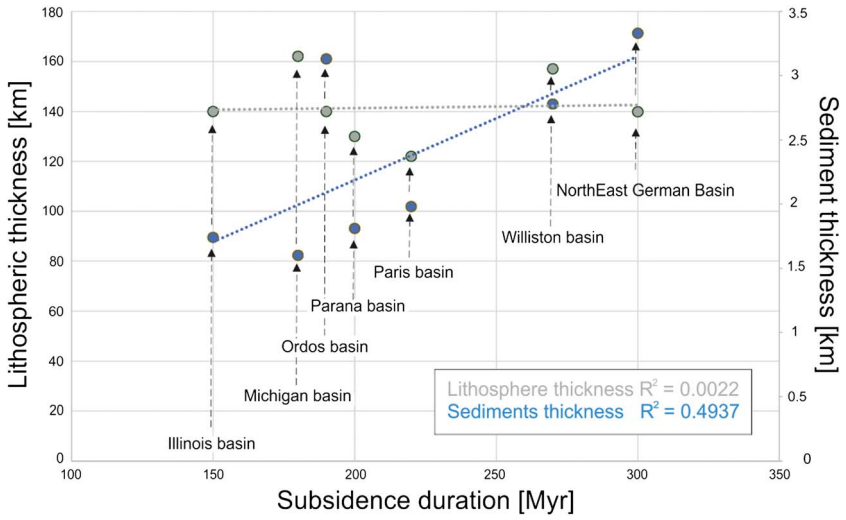

Figure 1. Schematic diagram illustrating the relationship between the duration of subsidence and the configurations of the lithosphere and of the sedimentary infill at specific intracontinental basins. Lithospheric thickness data are after *Artemieva* [2006], sediment thickness after *Heine et al.* [2012], and subsidence duration after *Xie and Heller* [2009]. The observed lack of correlation between equilibrium lithospheric thickness (grey circles) and subsidence duration strongly suggests that subsidence in these basins cannot be exclusively explained by differences in the initial lithospheric configuration of the respective basins. In contrast, preserved sediments thickness (light blue circles) provides a better fit to the duration of subsidence, thus supporting the existence of a dynamic and structural relation between sedimentation pattern and history and resulting subsidence history.

scale dynamics, an assumption that calls for caution when upscaling to the three-dimensional scale of sedimentary basins [*Petersen et al.*, 2010]. Only recently, there have been attempts to simulate the 3-D stratigraphic evolution during basin subsidence [*Braun et al.*, 2013]. However, these models mainly focus on feedback effects between surface dynamics and basin architecture whereas additional processes occurring in the deeper parts of the lithosphere are either missing or considered in a simplified manner.

We hypothesize that the mode of sediments accumulation typical of intracontinental basins and the long-term preservation of their stratigraphy are supportive of a system which has not attained a state of local isostatic equilibrium at any stage in its evolution. It is rather indicative of a dynamic system in which thermal and mechanical equilibrium between surface loading by sedimentation and thermal stresses by lithospheric cooling is achieved over geologic time by elastic-brittle-plastic stress relaxation within the lithospheric plate. To evaluate our hypothesis, we have developed 3-D thermomechanical models accounting for the feedback between sedimentation, rheology-dependent lithospheric flexure, and thermal contraction by lithospheric cooling; see Figure 2. Dynamic coupling is imposed in terms of a time and spatially varying flexural rigidity of the lithosphere taking into account both thermal and mechanical contributions (thermal and mechanical feedback loops of Figure 2). According to variations in the flexural rigidity of the plate, the deformation and subsidence of the basin varies in space and time and has an effect on the thermal and mechanical evolution of the model. Considering the details of these processes under their proper temporal and spatial scales leads to a complex evolution of the system in which changes in the internal configuration of the plate are related to the interplay between loading from sedimentation and thermal contraction of the initial thermal anomaly. When applied to conditions typical of intracontinental settings, our approach provides a coherent evolutionary model to explain their background subsidence by elucidating the mechanical and thermal processes driving their evolution. Based on the obtained results, we can therefore group intracontinental basins within the drift-rift suite of basins forming at low strain rates [*Armitage and Allen*, 2010], but we consider their prolonged subsidence as the direct consequence of the loading history of their sedimentary cover.

2. Methodology

2.1. Problem Formulation

We use a 3-D thermomechanical flexural model specifically designed to solve for the coupling between lithosphere scale conductive and advective heat transfer and flexural stresses from external and internal forcing

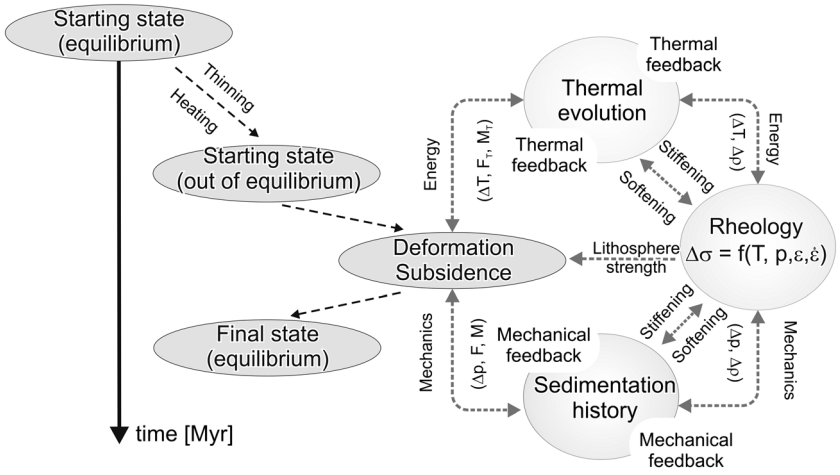

Figure 2. Thermomechanical processes and their feedback effects affecting the subsidence in intracontinental basins. An initial perturbation initiates a thermal anomaly in the deeper part of the lithosphere and moves the system out of thermal and mechanical equilibrium. This leads to the generation of internal stresses acting on the plate resulting from variations in the thermal configuration (ΔT) in the form of a net shear force (F_T) and a bending moment (M_T) as well as to changes in the rheological configuration of the lithosphere. Those variations trigger crustal deformation (subsidence and/or uplift), which retroaffects the thermal and rheological configurations, thus promoting new internal stresses and renewed lithospheric deformation (thermal feedback cycle). Sedimentation additionally affects the deformation history by imposing a direct load on the plate, by changing the strength of the lithosphere via the nonlinear rheological constitutive equations, and by retarding the cooling via thermal blanketing (mechanical feedback cycle).

(sedimentation/erosion, eustasy, and in-plane and thermal stresses). We parameterize the flexural rigidity of the lithospheric plate following the concept of the yield strength envelope (YSE) accounting for elastic, brittle, and plastic (secondary creep) rheology [*Burov and Diament*, 1995]. Surface deformation results from body forces acting on the plate due to sedimentation and internal variations in the thermomechanical configuration of the plate. The surface topography is updated according to the obtained deflection after each time step to follow the topmost surface of the youngest sediment unit. The bottom boundary of the model coincides with the lithosphere-asthenosphere transition and is here implemented as a thermomechanical boundary, the topology of which varies during the simulation in response to variations in the thermal and mechanical configuration of the plate. The thermal and flexural modules, described in the next paragraphs, are coupled via the temperature dependence of creep parameters and rock density, and the final system of equations is solved by an iterative approach during each time step.

2.1.1. Thermal Module

The governing equation solved for heat transport takes the following form:

$$(\rho c_p)\frac{DT}{Dt} = \nabla\cdot(k\nabla T) + H \tag{1}$$

In equation (1), ρ is the rock density, c_p is the isobaric heat capacity, T is the temperature, k is the thermal conductivity, H is the amount of heat produced within the rock by decay of radiogenic elements, and $\frac{DT}{Dt} = \frac{\partial}{\partial t} + v\cdot\nabla$ is the total (Lagrangian) derivative. Table 1 lists all thermal parameters adopted. We solve equation (1) by a finite element technique using bilinear cubic elements. The module integrates a full tensor representation of all material properties, and it accounts for the functional behavior on the resulting temperature conditions of mantle thermal parameters, namely, heat capacity [*Gilet et al.*, 1991], thermal expansion [*Berman and Brown*, 1985], and thermal conductivity [*Xu et al.*, 2004]. Equation (1) is solved via a parallel library package [*Nishida*, 2010] adopting an iterative restarted generalized minimal residual method (GMRES) with a dual threshold Incomplete Lower Upper (LU) matrix factorization (ILUT). Time integration is performed by a second-order accurate finite difference implicit (Crank-Nicholson) scheme with a posteriori upper bound.

2.1.2. Flexural Module

The mechanical response of a layered lithosphere to internal and external forcing is calculated by numerical integration of the boundary value problem described by the four first-order differential equations of mechanical equilibrium for a loaded plate [*Nadai*, 1963]. The total load acting on the plate consists of three major

Table 1. List of Thermal Properties[a]

Unit	Parameter	Symbol	Value	SI Units
Sediments	Thermal conductivity	K	2.0–2.2	$W\,m^{-1}\,K^{-1}$
[*Ranalli and Murphy*, 1987]	Isobaric heat capacity	c_p	0.8–1.0	$kJ\,m^{-3}\,K^{-1}$
	Heat production	H	0.0–0.01	$\mu W\,m^{-3}$
	Thermal expansion	α	0.0	$10^{-5}\,K^{-1}$
	Reference density	ρ	2400–2600	$kg\,m^{-3}$
Upper crust	Thermal conductivity	K	2.5	$W\,m^{-1}\,K^{-1}$
[*Gleason and Tullis*, 1995]	Isobaric heat capacity	c_p	0.8	$kJ\,m^{-3}\,K^{-1}$
	Heat production	H	0.9–1.2	$\mu W\,m^{-3}$
	Thermal expansion	α	3.28	$10^{-5}\,K^{-1}$
	Reference density	ρ	2700–2900	$kg\,m^{-3}$
Lower crust	Thermal conductivity	K	2.5–3.0	$W\,m^{-1}\,K^{-1}$
[*Rybacki and Dresen*, 2000]	Isobaric heat capacity	c_p	0.8	$kJ\,m^{-3}\,K^{-1}$
	Heat production	H	0.0–0.75	$\mu W\,m^{-3}$
	Thermal expansion	α	3.28	$10^{-5}\,K^{-1}$
	Reference density	ρ	2800–2900	$kg\,m^{-3}$
Lithospheric mantle	Thermal conductivity	K	[*Xu et al.*, 2004]	$W\,m^{-1}\,K^{-1}$
[*Hirth and Kohlstedt*, 2003]	Isobaric heat capacity	c_p	[*Gilet et al.*, 1991]	$kJ\,m^{-3}\,K^{-1}$
	Heat production	H	0.0	$\mu W\,m^{-3}$
	Thermal expansion	α	[*Berman and Brown*, 1985]	$10^{-5}\,K^{-1}$
	Reference density	ρ	3300	$kg\,m^{-3}$

[a]Different model realizations have been carried out without finding the general conclusions described in the main text being affected by such variance.

components: (1) an applied vertical load, q, which accounts for sedimentation/erosion and/or sea level variations; (2) a restoring force along the lower surface resulting from the buoyant behavior of the viscous asthenosphere material underneath. The latter is here implemented by a linear elastic Winkler foundation of module K, which imparts a normal traction to the base of the plate; and (3) a shear force $N=[N_{xx}, N_{xy}, N_{yy}]$, which takes into account in-plane and internal (gravitational and thermal) stresses. The resulting equations read as follows:

$$\nabla^2 M + \nabla(N\cdot\nabla\omega) - K\omega = q - \nabla(N\cdot\omega_0) \tag{2a}$$

$$M = \int(\Delta\sigma z)\mathrm{d}z' = -D\nabla^2\omega \tag{2b}$$

$$N = \int\Delta\sigma\,\mathrm{d}z' \tag{2c}$$

In equations (2a)–(2c), M is the plate bending moment ($\Delta\sigma$ being the internal state of stress (see below), z depth, D the flexural rigidity of the lithosphere, and $\nabla^2\omega$ the local radius of curvature of the bending plate); N is the shear force acting on the plate; ω is the plate deflection; and ω_0 is an initial vertical displacement for a stress-free (pre)loaded stage. In equations (2b) and (2c) integration is performed along the whole thickness of the rigid lithospheric plate.

Changes in the thermal configuration result in a residual 3-D density distribution according to the transient temperature at each time step (equation (1)), which gives rise to a body force acting on the lithosphere as

$$\Delta\rho = \int\Delta\rho(T,z)\mathrm{d}z' \quad \text{with} \quad \rho(T(z),z) = \rho_0(z)[1-\alpha(T)(T(z)-T_0(z))] \tag{3}$$

where ρ_0 and T_0 are the reference density and temperature at a specific depth, respectively, and α is the coefficient of thermal expansion. Integration is performed along the whole lithosphere thickness. From equation (3), it follows that additional horizontal and vertical variations in the thermal field initiate internal stresses, which are parameterized in the form of a thermal bending moment (M_T) and a thermal shear force (N_T) couple acting on the plate as

$$M_T = \alpha(T)E\int(zT(z))\mathrm{d}z' \tag{4a}$$

$$N_T = \alpha(T)E\int T(z)\mathrm{d}z' \tag{4b}$$

2.1.3. Rheological Module

The rheological model used to describe the mechanical response of a layered lithosphere to internal and external loads incorporates the temperature and stress dependence of rock material based on triaxial laboratory

measurements of rock-forming minerals [*Ranalli*, 1995]. We include the stress dependency following the concept of the yield strength envelope (YSE) by generalizing the approach described in *Burov and Diament* [1995] for a variable Young modulus, *E*, after *Tesauro et al.* [2013] and by taking into account details of the sedimentation history. In the current formulation, we neglect discrete faulting as it has been shown to result only in minor reduction of effective elastic thickness [*Kusznir and Karner*, 1985]. Additionally, it is likely that at low strain rates as considered in this study, deformation does not tend to focus along large discrete faults but shows a more diffusive behavior [*Armitage and Allen*, 2010].

We model the (quasi) elastic behavior of the lithosphere by assuming infinite strain rates at finite stress values as

$$\Delta\sigma^{\mathrm{el}} = \frac{E}{1+\nu}\left(\epsilon_{\mathrm{el}} + \frac{\nu I_2}{1-2\nu}\right) \tag{5}$$

where E is the Young modulus, ν the Poisson's ratio, and $I_2 = \epsilon_{ii}\epsilon_{jj} - \epsilon_{ij}\epsilon_{ij}$ the second invariant of the elastic strain.

Depth-dependent yield stresses are determined by combining the concept of rock frictional strength with a yield stress for solid-state creep. Pressure-sensitive brittle rock behavior is introduced in terms of a variant of Mohr-Coulomb plasticity, usually referred to as Byerlee's law [*Ranalli*, 1995] as

$$\Delta\sigma^{b} = c_f \rho(T) g z (1-\lambda) \tag{6}$$

where c_f is the friction coefficient, $\rho(T)$ is the rock density, g is the acceleration due to gravity, z is the depth of the bottom of the layer, and λ is the mean hydrostatic pore fluid factor, defined as the ratio of pore fluid pressure to overburden pressure.

Steady state, secondary creep is implemented as a combination of thermally activated power law describing dislocation creep and dislocation glide (Dorn's law) for olivine at differential stresses higher than 200 MPa:

$$\Delta\sigma^{d} = \begin{cases} \left(\dfrac{\dot{\epsilon}}{A}\right)^{\frac{1}{n}} e^{\left(\frac{H}{nRT}\right)} & \text{if } \Delta\sigma^{d} < 200 \text{ MPa} \\ \sigma_0 \left(1 - \left[-\dfrac{RT}{Q}\ln\left(\dfrac{\dot{\epsilon}}{\dot{\epsilon}_0}\right)\right]^{\frac{1}{2}}\right) & \text{if } \Delta\sigma^{d} > 200 \text{ MPa} \end{cases} \tag{7}$$

with $\dot{\epsilon}$ being the strain rate, A the power law strain rate, n the power law exponent, H the activation enthalpy, R the gas constant, T temperature, σ_0 Peierls critical stress, Q Dorn activation energy, and $\dot{\epsilon}_0$ Dorn critical strain rate.

The strength of the plate results from the relative contribution of pressure-sensitive brittle behavior and thermally activated but strain rate-invariant secondary creep deformation at depths. Therefore, our rheological model likely overestimates the long-term lithospheric strength. This behavior could be in principle modulated by accounting for viscous softening within the ductile domain of the plate [*Albert et al.*, 2006; *Huismans and Beaumont*, 2011], though there are some concerns on the physical derivation of usually adopted weakening laws [*Regenauer-Lieb et al.*, 2006]. Therefore, lithospheric strength as calculated by our approach should be considered as representing an upper bound.

2.1.4. Iterative Solution Approach

The YSE is computed by combining the constitutive rheological equations (5)–(7) and by taking into account the current temperature configuration as determined by solution of equation (1). We calculate the YSE at every point in the mesh, such that the internal stress state and deformation due to loading are based on the *p-T* conditions at the given point. Under the assumption of constant strain rate, the transition from frictional slip to secondary creep occurs at the interception point between the frictional plastic and creep yield stress. Therefore, our approach does not permit consideration of semibrittle deformation [*Evans et al.*, 1990]. The resulting YSE is used to compute the flexural deformation by solving equations (2a)–(2c) with additional thermal stresses as described by equations (3), (4a), and (4b). The state of stress in the lithospheric plate depends on the thermal configuration of the lithosphere, on the lithostatic pressure field, and on the curvature of the bending plate. Constitutive relationships among these quantities are nonlinear, and they result in a nonlinear bending moment-plate curvature relation. We linearize the problem by a classical Newton-Raphson iteration algorithm at each time step. The procedure works as follows. (i) It starts by finding a trial state of

bending ($\omega^{trial} = \omega^{el}$) via a linear, purely elastic solution to equation (2a), given a certain rigidity distribution, D^{trial}. (ii) It then determines the stress distribution ($\Delta\sigma = \min(\Delta\sigma^{el}, \Delta\sigma^{b}, \Delta\sigma^{d})$) according to the internal thermal state and the trial solution computed at the previous stage. (iii) The bending moment (M) and the equivalent shear force (N) acting on the plate are then updated based on the newly computed stress distribution (via equations (2b) and (2c)). (iv) The bending moment together with the curvature radius derived from the previous iteration are used to "correct" the flexural rigidity of the lithosphere (right term in equation (2b)), which is then used to update the deflection based on the current load state and stress distribution by solving equation (2a). The newly computed deflection is input in stage (ii), and the coupling cycle (from (ii) to (iv)) is reiterated until a convergence is obtained in the computed flexural rigidity; that is, the magnitude of the square norm error between two consecutive iteration steps is less than a threshold value imposed. Thermal feedback effects are explicitly considered in that the thermal state of the system is updated after each iteration by solving for equation (1). Thermal stresses are then added to the bending moment and shear force (equations (4a) and (4b)) prior to solving for the flexure equation (2a). At the end of each successful iterative cycle, a new model configuration is obtained, which is consistent with the current thermal and mechanical internal states.

At each iteration, the linearized system is solved relying on a high-order finite difference scheme (modified 13-point stencil approximation with second-order truncation error). The iterative solution is achieved via a multigrid solver based on a Gauss-Seidel smoothing operator and a red-black ordering of the grid points as restriction/prolongation operator within a W cycle (4-4-16) to accelerate convergence.

2.2. Initial Model Setup and Boundary Conditions

We have applied the numerical framework as described in the previous paragraphs to model the subsidence history at generic-type intracontinental settings. Whether some cratonic basins overlie old, cold, and therefore thick Precambrian continental lithosphere (e.g., Congo basin, Hudson Bay basin, and West Siberian basin), others overlie much younger (Phanerozoic) continental lithosphere (e.g., Paris basin and North German basin). In order to account for this observed variability, we have run several models in terms of the equilibrium lithospheric configuration considered. For the sake of clarity, we here present two end-member scenarios. We first discuss the results from a model that considers a lithospheric thickness of 150 km (reference model) as representative of post-Cambrian intracontinental settings. The results obtained based on an equilibrium thickness of 200 km, representative of cratonic basin configurations, are discussed later in the manuscript. Figure 3 schematically illustrates the model geometry together with the boundary and initial conditions imposed. We consider a stratified lithosphere consisting of an upper and a lower crust overlying a lithospheric mantle of variable thickness overlying a viscous asthenosphere. For all model realizations, we have also varied the basic assumed rheology and thermal properties of all layers of the lithosphere within observational constraints from laboratory measurements as summarized in Tables 1 and 2, without finding our results being affected by such variations.

The thermal boundary condition imposed across the topmost surface consists of a fixed (first kind) temperature, $T = 0$°C. As described in the previous paragraph, we regard the lithosphere as a purely conductive plate. Therefore, we do not attempt to model any convective process that might occur in the deeper mantle, i.e., small-scale convection. However, their effects have been implicitly taken into account by imposing a constant heat input thermal boundary condition along the base of the model [*Doin and Fleitout*, 1996]. For the two model realizations presented later in the manuscript, its value has been fixed to 25 mW m^{-2} and 20 mW m^{-2}, consistent with an equilibrium thermal thickness of the lithosphere of 150 km and 200 km, respectively. We model the transition from the rigid conductive mantle lithosphere to the viscous isoentropic asthenosphere (LAB transition in Figure 3) by means of an isotherm, i.e., $T = 1300$°C. Results obtained from simulations with a different isotherm (tested values in the range 1200–1400°C) did not produce changes in the overall subsidence evolution. We do not fix this boundary a priori. Indeed, it varies in time according to the thermal and mechanical configuration computed at each time step, and we keep track of its position throughout the simulation via history-dependent particle markers [*Moresi et al.*, 2003].

Symmetry boundary conditions (zero-normal deflection and tangential traction) are enforced along the four model boundaries, and a restoring force is applied across the base of the model (LAB transition). It is implemented via a Winkler foundation of module $K = g\Delta\rho = g(\rho_a - \rho_i)$, with ρ_a being the density of the asthenosphere and ρ_i the density of the infill material. The latter represents the transition from the solid part of the lithosphere to the viscous asthenosphere. Topographic loading by sedimentation is introduced in the model by assuming continuous sedimentation as soon as new accommodation space is made available. Therefore, the thickness

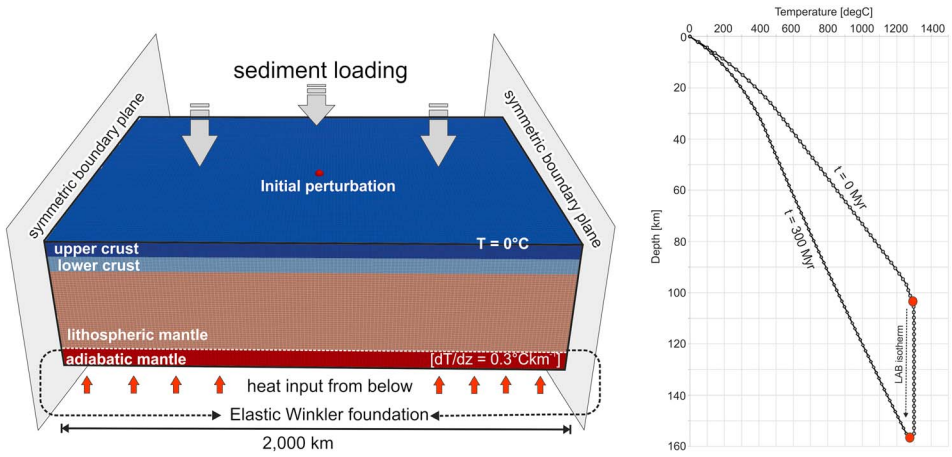

Figure 3. Model setup, initial and boundary conditions for modeling the subsidence history at a generic-type intracontinental basin. (left) The lithosphere (variable thickness ranging between 150 km and more than 200 km) consists of a two-layered crust and a lithosphere mantle layer overlying an adiabatic mantle domain (here integrated to set proper boundary conditions for the thermomechanical model). Also shown are the boundary conditions adopted. The surface temperature is kept fixed at $T = 0$°C. A constant basal heat flow is imposed along the base of the model. Its value has been chosen in order to be consistent with the equilibrium thermal thickness of the lithosphere considered at each simulation. It ranges between $q = 25$ mW m^{-2} for the case of a plate thickness of 150 km and $q = 20$ mW m^{-2} for a 200 km plate thickness configuration. (right) Temperature profiles taken at a single point in the center of the domain (red point in Figure 3, left) illustrating the thermal destabilization imposed in order to initiate the subsidence. Its magnitude has been based on the thermal configuration as derived from a 1-D uniform stretching model approximation, and it can be therefore parameterized in terms of the stretching factor (β). The temperature profile at the same location as extracted from the 3-D model after approximately 200 Myr of thermal cooling is also shown.

of the sedimentary infill varies in time as a function of the amount of surface deformation and is limited by the $z = 0$ isosurface; that is, no erosion is considered in the present case. This is consistent with both the slow rates of sediments supplied and the high preservation potential of these settings, observations suggesting how erosional processes likely play a minor role for the stratigraphic evolution of these settings and, therefore, for their subsidence history. For the simulations presented in the following of the manuscript, active sedimentation spans an interval of 150 Myr, with all sediments sharing the same set of thermal and mechanical parameters. We let the system equilibrate for a longer period (350 Myr). This is done in order to examine the effects of the final load distribution on the long-term stress and thermal configuration of the plate.

The geodynamic context during the origin of intracontinental basins is suggestive of large-scale extensional dynamics, possibly interacting with mantle plume activity. Indeed, classification schemes of intracontinental basins generally associate the subsidence evolution of these settings to continental stretching followed by flexural compensation and lithospheric cooling of the initial thermal perturbation [*Armitage and Allen*, 2010]. Therefore, cooling of the thermal anomaly induced by mechanical stretching and/or plume dynamics has a fundamental role in the origin and evolution of these basins. The purpose of this work, however, is not to model details of the rifting dynamics leading to a thermally destabilized lithosphere. We rather aim at illustrating how, by properly considering the interactions between lithospheric cooling and sedimentation, it is possible to explain the long-term, postrift subsidence evolution of intracontinental basins. Therefore, it seems justifiable to use a simplified kinematic representation of the initial perturbation driving the subsidence as described in the following, by considering the consequent limitations while interpreting the obtained results.

We perturb the initial model configuration by imposing a thermal anomaly in the deeper lithosphere located in the central domain of the model area (indicated by the red point in Figure 3). Though aware that there might be several mechanisms that can account for a thermal destabilization of the lithosphere (e.g., mantle delamination, mechanical stretching, and plume intrusion), we have resorted to the rather simple concept of one-dimensional pure-shear, uniform stretching [*McKenzie*, 1978] to parameterize both the magnitude and the vertical extension of the anomaly. We have opted for this approach because of its inherent simplicity to describe the model configuration by means of a single dimensionless parameter, namely, the stretching/thinning factor (β factor hereafter). Other authors have discussed potential effects of finite

Table 2. List of Rheological Properties[a]

Unit	Parameter	Symbol	Value	SI units
Sediments	Reference density	ρ_0	2400–2600	$kg\,m^{-1}$
[*Ranalli and Murphy*, 1987]	Power law exponent	n	2.72–3.3	(-)
	Power law strain rate	A	9.98×10^{-32} to 3×10^{-26}	$Pa^{-n}\,s^{-1}$
	Activation enthalpy	H	102–186	$kJ\,mol^{-1}$
	Friction coefficient (extension)	c_f	0.75	(-)
	Friction coefficient (compression)	c_f	3	(-)
	Pore fluid factor	λ	0.36	(-)
Upper crust	Reference density	ρ_0	2700–2900	$kg\,m^{-1}$
[*Gleason and Tullis*, 1995]	Power law exponent	n	2.4–3.1	(-)
	Power law strain rate	A	2.01×10^{-21} to 1.26×10^{-16}	$Pa^{-n}\,s^{-1}$
	Activation enthalpy	H	134–186	$kJ\,mol^{-1}$
	Friction coefficient (extension)	c_f	0.75	(-)
	Friction coefficient (compression)	c_f	3	(-)
	Pore fluid factor	λ	0.36	(-)
Lower crust	Reference density	ρ_0	2800–2900	$kg\,m^{-1}$
[*Rybacki and Dresen*, 2000]	Power law exponent	n	2.72–3.3	(-)
	Power law strain rate	A	9.98×10^{-32} to 3.0×10^{-26}	$Pa^{-n}\,s^{-1}$
	Activation enthalpy	H	243–445	$kJ\,mol^{-1}$
	Friction coefficient (extension)	c_f	0.75	(-)
	Friction coefficient (compression)	c_f	3	(-)
	Pore fluid factor	λ	0.36	(-)
Lithospheric mantle	Reference density	ρ_0	3300	$kg\,m^{-1}$
[*Hirth and Kohlstedt*, 2003]	Power law exponent	n	3.6	(-)
	Power law strain rate	A	7.94×10^{-18}	$Pa^{-n}\,s^{-1}$
	Activation enthalpy	H	510	$kJ\,mol^{-1}$
	Friction coefficient (extension)	c_f	0.75	(-)
	Friction coefficient (compression)	c_f	3	(-)
	Pore fluid factor	λ	0.36	(-)
	Peierls critical stress	σ_0	8.5×10^{9}	Pa
	Dorn activation energy	Q	535	$kJ\,mol^{-1}$
	Dorn critical strain rate	$\dot{\epsilon}$	5.7×10^{11}	s^{-1}

[a]Different model realizations have been carried out without finding the general conclusions being affected by such variance.

[*Armitage and Allen*, 2010] and depth-dependent strain rates [*Huismans and Beaumont*, 2011]. However, for the range of strain rates tested $\left(\dot{\epsilon} \div \left[10^{-14} - 10^{-17}\right] s^{-1}\right)$, we did not find our conclusions to be overall affected by variations in these parameters.

To generate the initial thermal anomaly, we have calculated the amount of passive raising of the LAB 1300°C isotherm as resulting from homogenous thinning of the crust and of the mantle lithosphere under an imposed β factor, based on a 1-D column of the lithosphere extracted from the 3-D model. This is schematically illustrated in Figure 3 (right). The β factor imposed, therefore, does not imply any active mechanical extension in a strict sense but is rather intended to parameterize the thermal perturbation to the initial lithospheric configuration. The range of variations of β factors considered in the study has been chosen to model postrift conditions typical for intracontinental settings. Stretching factors derived either from preserved crustal thickness and/or from reconstructed tectonic subsidence curves rarely exceed a value of $\beta = 1.5$ [*Gac et al*., 2012; *Heine et al*., 2012; *Pawlak et al*., 2011]. Therefore, we gradually increase its value from a minimum of $\beta = 1.1$ up to a maximum of $\beta = 1.5$. To guarantee stability of the numerical solution, we opted for a smoother variation in the LAB isotherm from the unperturbed and perturbed domains. Accordingly, we impose a gradual transition of the thermal anomaly within an area of finite extent centered on the point of maximum thermal destabilization (marked in red colors in Figure 3). Our choice for the initial setting is consistent with the typical bull's eye pattern of the stratigraphy of the infilling sequences observed in many intracontinental settings worldwide [*Sloss*, 1988; *Scheck and Bayer*, 1999]. Therefore, we support the hypothesis that the outline of these basins is a syndepositional feature. The geometry of the imposed thermal anomaly is 10 km by 5 km in horizontal extension(x and y axes, respectively). We impose a slight asymmetry in the geometry of the imposed thermal anomaly to represent a preferential axis of deformation, as induced by a small in magnitudes extensional tectonic regime at the time of basin formation.

Based on the newly generated topology of the LAB, an initial steady state simulation has been carried out in order to derive the corresponding thermal configuration used as initial condition for the modeling stage. The mechanical state of the system at the starting of the modeling has been derived based on a lithostatic stress distribution according to the geometry and thermal boundary setting imposed. Starting from this initial thermomechanical state, the system is let to cool down the initial thermal anomaly (see Figure 3), thus giving rise to a phase of subsidence that will be discussed in the next paragraph.

3. Results

3.1. Reference Model

In Figure 4a we compare the thermal subsidence as extracted from a 3-D model which considers (dashed curves) and a model which neglects (continuous curves) the presence of the sedimentary cover. Both models have the same set of rheological and thermal parameters (see Tables 1 and 2). In the latter case, the system converges quite rapidly, with a diffusive time scale of approximately 100 Myr, toward a condition of thermal equilibrium. From this time onward, it shows a long-term, exponentially decaying subsidence, which tails off asymptotically. The modeled diffusive time scale of the process is in the range of that considered typical both for oceanic and stable continental conditions [*McKenzie*, 1978; *Stein and Stein*, 1992]. Thermal and mechanical effects of sediments on a thermally relaxing lithosphere affect the subsidence evolution through time significantly. Indeed, subsidence curves follow a quasi-linear trend, without approaching any asymptotic, long-term value. Not surprisingly, this effect is more pronounced for larger thinning factors ($\beta \geq 1.2$). Interestingly, the presence of the sedimentary cover affects the subsidence pattern even long after active sedimentation ceases (post sedimentation subsidence in Figure 4a). This aspect points to a lithosphere that is able to preserve a thermomechanical memory of its previous history, thereby forcing the internal thermal and mechanical configuration to lag behind the actual basin architecture.

The results discussed above can be better understood in terms of induced variations in the flexural strength of the lithosphere by active sedimentation. Figure 4b shows the evolution through time of the flexural rigidity of the lithosphere (D) normalized by its value at the onset of cooling. In both cases, D increases with time in a consistent manner as constrained for both oceanic and continental lithosphere [*Burov and Diament*, 1995; *Kusznir and Karner*, 1985]. The nonlinear temporal behavior of the flexural strength results from the nonlinear rheological response of the system to variations in the thermal field and loading history. When no sedimentation is considered, the flexural rigidity first increases quite rapidly (first stiffening phase from ~30 Myr to ~100 Myr), and then it stabilizes toward an asymptotic value (stress decay stage as indicated by the final plateau at around 150–200 Myr in the curves of Figure 4b). Loading by sediments weakens the lithosphere, which is characterized by a smaller flexural strength when compared to the no-sediment case. On the one hand, weakening of the lithosphere results from thermal blanketing by sediments that leads to increased lithospheric temperature. On the other hand, loading by sediments promotes additional weakening of the lithosphere by reducing the lithostatic state of stress within the plate (mechanical feedback effect). In addition, as sediments are added to the lithosphere, rates of variation in flexural rigidity significantly drop, though the latter still increases with time. As a result, during the first 350 Myr the lithosphere undergoes only minor mechanical stiffening without showing any stabilization by stress decay at mantle level. Results from simulations protracted in time restrain mechanical stabilization to occur within a time range from 600 Myr (150 km case) up to 800 Myr (200 km case).

The main contribution to the variations in the flexural rigidity arises from the transient thermal configuration of the lithosphere and its interdependency to the loading history, i.e., thermomechanical effects of lithospheric cooling and sedimentation. Early in the postrift evolution, the evolution of the subsidence is a function of the rheology of the crust. Therefore, the duration of this first stage is constrained by the ability of crustal rocks to contract the initial thermal anomaly and can be parameterized in terms of crustal thermal diffusivity. Rapid cooling of the crust not disturbed by overlying sediments initiates a phase of rapid subsidence as depicted in Figure 4a. As the crust cools, it also increases its flexural strength and, consequently, its ability to support loads. Therefore, cooling of the crust during early stages is also associated with an increase in the flexural strength of the plate, thus giving rise to a first phase of flexural stiffening (Figure 4b). Due to its lower thermal decay constant, and to the internal contribution of heat from radioactive decay, the crust stabilizes faster than the deeper mantle. When sedimentation is neglected, this happens approximately around 100 Myr, while considering the presence of sediments, crustal stabilization is delayed by approximately 100 Myr (see in addition section 4).

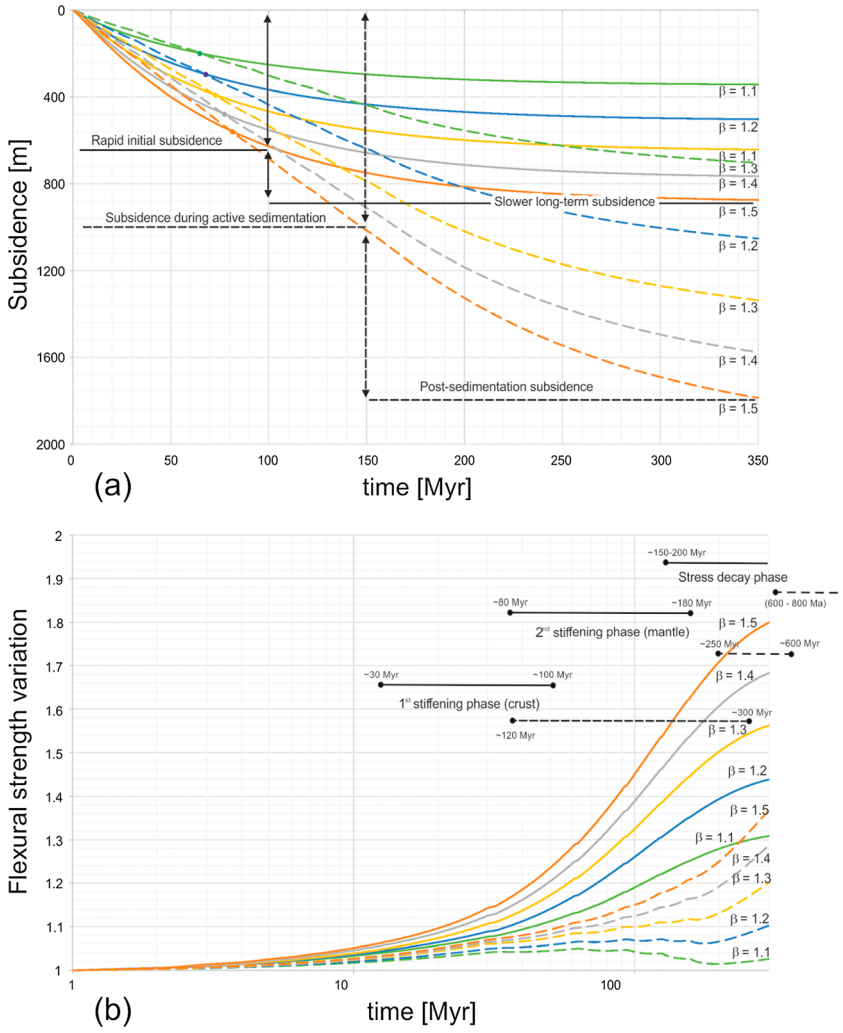

Figure 4. Effects of the sedimentary cover on the long-term subsidence and flexural strength of continental lithosphere. (a) Comparison between thermal subsidence curves for a no-sediment case (solid curves) and a case with active sedimentation (dashed curves). In the former case, thermal subsidence curves show an exponential decay in time, therefore similar to the pattern predicted by a plate-cooling model. The presence of sediments induced a prolonged in time and slower thermal subsidence, thus resembling the first-order characteristics as observed in intracontinental settings. (b) Variations in the flexural rigidity of the plate as a function of time, normalized by its value at the onset of cooling. Dashed curves refer to a case where sedimentation is considered and continuous curves to a case where sediments are neglected. For all stretching factors considered, the presence of a sedimentary cover results in overall relatively smaller flexural rigidities. In all figures, different colors refer to different β factors considered to parameterize the thermal anomaly at the onset of cooling.

From this time on, the strength of the mantle continues to increase (giving rise to a second stiffening phase as depicted in Figure 4b) while the crust has already stabilized. Because of this new thermomechanical configuration, the flexural strength of the plate grows further, but subsidence is slower. The rheological constraints imposed on calculating the flexural strength of the plate impedes the mantle strength to grow indefinitely. Indeed, reaching temperatures of about 700°C, thermally activated creep causes a stress decay in the mantle. The interplay between the thermal evolution of the lithosphere and stress decay in the mantle leads to a final stable thermomechanical state of the lithosphere characterized by a strength which is tailing off asymptotically to a constant value (stress decay phase of Figure 4b) and an asymptotic subsidence behavior (slower long-term subsidence in Figure 4a). Crustal thinning likely accelerates this behavior. This is because thinning of the crust lowers the amount of heat produced internally by radiogenic decay, thus providing additional cooling. However, when considering realistic rheology for the lithosphere, this effect is of only secondary importance relative to stress decay due to temperature activated creep. Additionally, given the low stretching factors

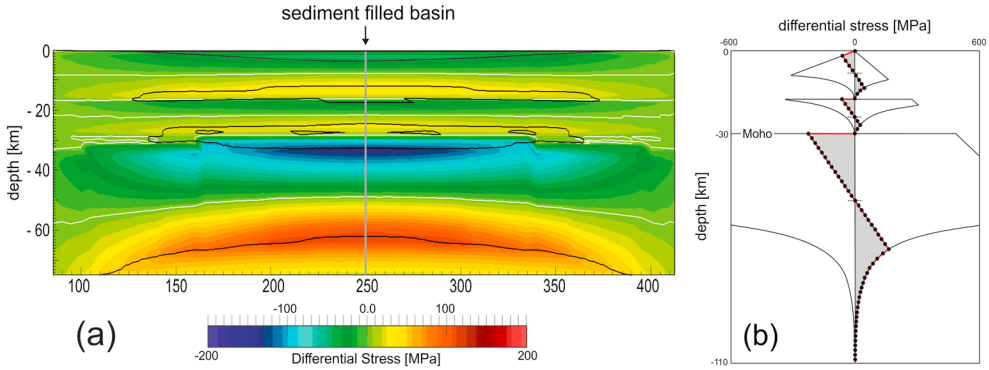

Figure 5. Effects of loading by sediments on the mechanical configuration of the lithosphere. (a) Differential stress distribution after 150 Myr of simulation time. White curves indicate the locations of neutral flexural planes (no differential stress) at different depths. Black lines contour the extent of the domains of plastic yielding (brittle or ductile creep) due to either tensile (positive) or compressive (negative) stresses. (b) Yield strength envelope (YSE) and bending stress distribution (shaded areas) at the point of maximum bending. Thermal and mechanical effects of the sedimentary cover result in a ductile weakening of the lower crust and in a decoupling of the lithosphere across the crust-to-mantle level. This is indicated by the high values of shear stresses and by a reversal of their signs (from compression to extension) at this depth. Due to crustal-mantle decoupling, each layer behaves mechanically independently and show a separate distribution of bending stresses. Stress decay due to thermally activated olivine creep occurs at depths greater than 80 km.

considered ($\beta \leq 1.5$), variations in radiogenic heat produced within the crust only slightly influence the subcrustal temperature distribution, thus having a minor role in affecting the mechanical properties of the lithosphere [*Kusznir and Karner*, 1985; *Kusznir*, 1982].

Due to their low value of thermal conductivity, the presence of sediments slows lithosphere cooling and therefore results in less initial subsidence when compared to the nonsediment case (Figure 4a and section 4) and in a delayed stiffening of the lithosphere (Figure 4b). Additionally, the amount of heat retained within the blanket causes a reduction in the yield stress within the upper crust (i.e., at the base of the infill). This further delays lithospheric stiffening, thus explaining the observed differences in the flexural strength of the plate under loading and unloading conditions (Figure 4b). At the same time, loading by sediments increases the Moho depth, thus raising lower crustal temperatures. This, in turn, promotes weakening of the lower crust, and it might finally lead to a crustal-mantle decoupling (Figure 5). In our formulation, mechanical decoupling between the crust and the lithospheric mantle arises spontaneously from thermomechanical feedback effects between the lower crust and upper mantle layers. Under these conditions, the upper mantle evolves into the stress-bearing part of the lithosphere (Figure 5b). Crust-mantle decoupling substantially lowers the lithospheric flexural strength, thus explaining the relative minor stiffening depicted in Figure 4b. Within a weak lithosphere, which cools at slower rates with respect to the case where sedimentation is neglected, mechanical stabilization due to stress decay in the mantle is delayed as well thus giving rise to a relatively slow thermal subsidence prolonged over geological times.

3.2. Influence of Equilibrium Plate Thickness

Differences in the equilibrium plate thickness may induce detectable variations in both the thermal and rheological configurations of the lithosphere. Therefore, they likely affect the long-term subsidence history. It has long been recognized that differences in the duration of thermal subsidence between oceanic and continental lithosphere can be explained in terms of differences in the thickness of the respective plates [*Burov and Diament*, 1995; *Stein and Stein*, 1992]. One-dimensional solutions to the plate-cooling problem constrain relaxation constants up to 600 Myr for a plate thickness of 200 km or more with temperature changing approximately linearly within this time window. However, when accounting for the additional effect of sediments, predicted subsidence curves from one-dimensional approaches show too steep linear trends and result in an overfilled basin as not commonly observed in intracontinental settings. At the same time, as the strength of the plate increases with time during cooling, deviations from local isostatic compensation become more and more important. The main limitation of these analytical approaches is that they neglect the effects of time-varying sedimentation on the resulting thermal configuration and on the total strength of the plate during the evolution of a basin. To quantify these effects, we have carried out a sensitivity study

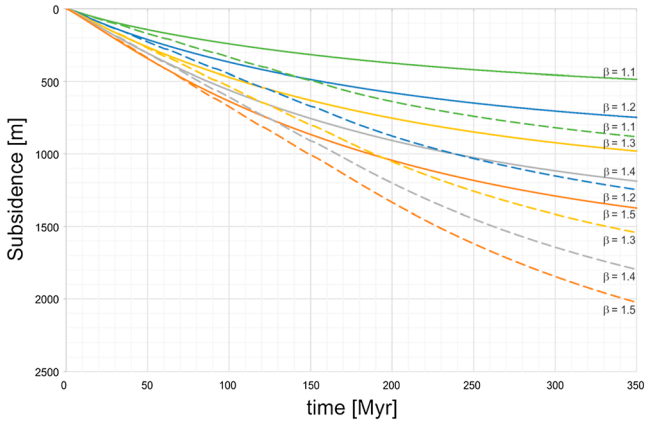

Figure 6. Effects of the internal lithospheric configuration on the resulting subsidence. Subsidence curves for a 200 km equilibrium plate thickness configuration (dashed curves) are compared to those obtained from the same model realization but considering a 150 km equilibrium thickness of the lithosphere (solid curves).

in which we have gradually varied the equilibrium thickness of the plate and have investigated its effects on the resulting long-term thermal subsidence. Figure 6 illustrates the modeled subsidence for a plate thickness of 200 km, as considered representative for Archean craton conditions [*McKenzie and Priestley*, 2005]. Thinning of an initially thicker and, therefore, denser lithosphere results in increased amounts of subsidence compared to the 150 km thick plate. In addition, even when the retarding effect of the sediments is neglected, calculated subsidence curves span longer times. The main effect of adding sediments is to slow down subsidence rates further. For high mantle to crustal thickness ratios, the integrated strength of the plate is primarily controlled by the strength of the competent mantle layer, while the crust contributes only secondarily to the mechanical strength of the plate. The sensitivity of mantle rocks to temperature variations makes it possible to describe the mechanical evolution in terms of variations in the thermal configuration of the plate alone. The relatively high diffusive time scales of the mantle lithosphere (>150 Myr) hinder rapid stabilization of the deeper geothermal field, which is less affected by surficial temperature conditions. This is turn leads to an unsteady mechanical configuration, which can explain the observed prolonged subsidence.

Therefore, the longevity of subsidence (lasting more than 200 Myr) seems plausible for certain ranges of plate thicknesses (~200 km or more), and it can be reasonably well explained in terms of processes occurring within the upper mantle. On the other hand, for other plate thickness configurations, prolonged subsidence cannot be fully reconciled if the retarding effects of the sedimentary cover is not properly accounted for. However, whether a trade-off exists among these parameters and what geodynamic implications it may imply remain only speculative at this stage.

4. Discussions

4.1. The 3-D Subsidence Analysis

So far, the results from the modeling have been mainly discussed in terms of one-dimensional subsidence profiles as extracted from the 3-D model. We have opted for 1-D profiles since they offer a clear and easy representation of the modeled subsidence history, and they permit, at the same time, to carry out a direct comparison between our results with those obtained from one-dimensional and two-dimensional model approximation as presented by other studies. In this section, we describe and discuss in some details the full three-dimensional expression of the processes investigated. Figure 7a illustrates in planar view the temporal evolution of the basin morphology (i.e., the total area that underwent deformation) and the thickness distribution of its infill as well as the final 3-D geometry of the basin cross-plotted on the computed temperature distribution at the end of the simulation, after 350 Myr. The results correspond to an equilibrium thickness of 150 km, initially perturbed by a thermal anomaly associated with β factor of 1.5.

The basin has an elliptical shape in planar view, preferentially elongated along the x direction. The major semiaxis is approximately 250 km, and the minor one around 150 km. The resulting surface area is approximately $A = 0.15 \times 10^6$ km^2, thus being in the range of sizes typically observed in intracontinental settings [*Klein and Hsui*, 1987]. The results obtained by considering an equilibrium thickness of 200 km show a similar geometry, though with a larger total area ($\div 2.3 \times 10^6$ km^2). The 3-D geometry of the basins is also compatible with those observed in natural examples, showing a typical saucer-shaped geometry, dipping rather gently toward the center of the basin [*Armitage and Allen*, 2010].

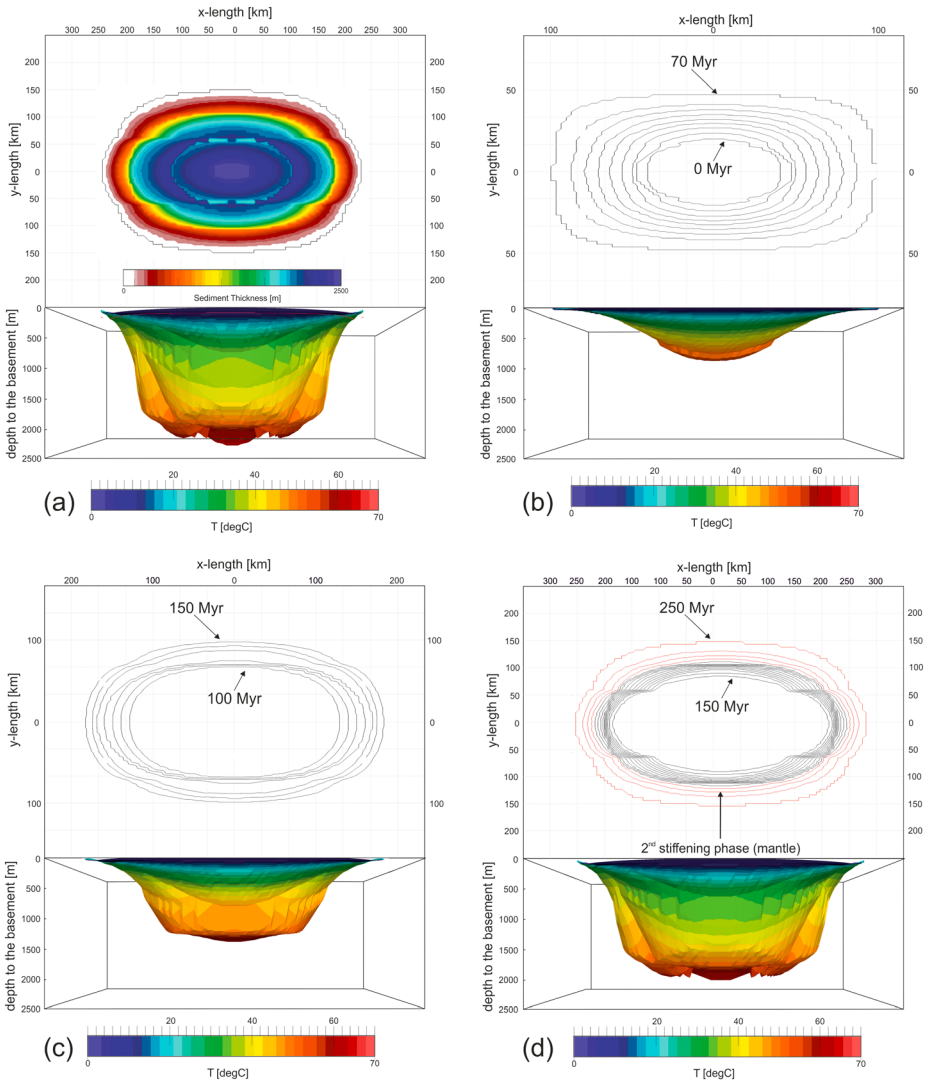

Figure 7. The 3-D subsidence history (150 km equilibrium thickness) at specific times in the evolution of the system. Each figure shows in planar view the temporal evolution of the area undergoing subsidence (top) and the final 3-D geometry of the basin, color coded by the thermal configuration across the basement (bottom). (a) End of simulation, $t = 350$ Myr. (b) Early subsidence stage in the evolution of the system, $t \div [0–70]$ Myr. (c) Stiffening phase at crustal level—end of sedimentation, $t \div [100–150]$ Myr. (d) End of sedimentation—beginning of stiffening within the mantle, $t \div [150–250]$ Myr.

In what follows, we discuss the 3-D evolution of the basin based on a description of the 3-D geometry at different times. For the sake of simplicity, we have subdivided our discussion into three main stages, marked by major changes in the evolution of the basin (Figures 7b–7d). Each figure illustrates the temporal evolution of the areas undergoing deformation in planar view (top), together with the basin 3-D geometry at the end of each stage, color coded by the temperature configuration at the base of the infill (bottom).

Early Subsidence Stage (0–70 Myr) (Figure 7b). During the initial phase in the evolution of the system, here limited by the beginning of flexural stiffening in the crust, subsidence is roughly radially symmetric, decreasing with distance from the basin center, located on top of the initial thermal anomaly. These observations point to thermal contraction by mainly crustal, diffusive processes as the major mechanism for the observed subsidence of the basin. Cooling of the crust, disturbed by active sedimentation, is the main cause of the modeled subsidence. Due to thermal blanketing by overlying sediments, the crust has not yet stabilized (see also Figure 4b), and the subsidence is controlled by the ability of crustal rocks to thermally contract the initial anomaly.

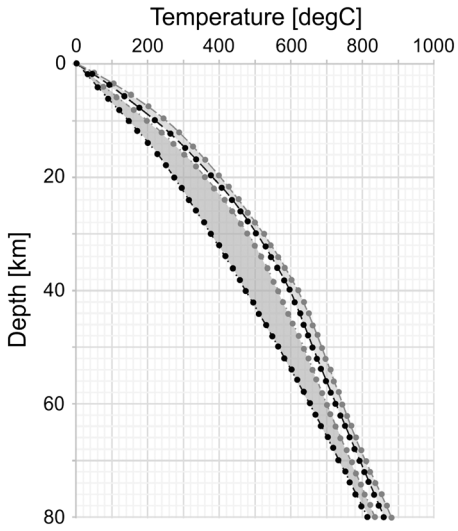

Figure 8. Temperature profiles as extracted from the 3-D model. Two different time steps are illustrated, that is, at the early stage ($t \sim 100$ Myr, that is, approximately when stiffening within the crust starts, dashed curves) and at a later stage (around 150 Myr, approximately when the crust starts relaxing accumulated stresses, dash-dotted curves). Black colors indicate the case where sediments are neglected, and grey colors the case when active sedimentation is considered. The grey areas highlight the difference in heat stored in the system at the different stages between the two model realizations.

First Stiffening Phase—End of Sedimentation (100–150 Myr) (Figure 7c). As the lithospheric strength increases with time, the subsidence pattern changes as does the shape of the basin. Stiffening at crustal level distributes the subsidence over a broader area within a shorter time with respect to the previous case. Because of the stiffening, the flexural wavelength of the deformation also increases. The basin area increases by approximately 70% within a time window of ~50 Myr, consistent with the observed increase (D being approximately 1.2 times its initial value) of the flexural strength of the plate during the same amount of time. In addition, the basin geometry loses the previously observed radial symmetry, a clear indication that both subsidence rates and basin geometry are highly affected by the loading history. Indeed, subsidence is now a nonlinear function of the thermal and mechanical configuration of the basin and results from the dynamic balance between thermal diffusion at mantle level (the crust having gradually stabilized), sediment loading, and related variations in the flexural stiffness of the plate, i.e., thermomechanical feedback effects.

End of Sedimentation—Second Stiffening Phase (150–250 Myr) (Figure 7d). The end of sedimentation marks the beginning of a new phase in the subsidence evolution as indicated by a growing pattern of the basin area (black colored curves). Despite the fact that sedimentation has ceased, the basin grows following a geometric pattern similar to that described for the previous stage. This is a clear indication that the previous history can imprint the future thermomechanical state of the basin. Crust-mantle decoupling (red colored curves) marks the onset of a different phase in the subsidence history. While the crust has stabilized, the mantle stiffens and gradually starts to bear the bulk of stress exerted on the plate. Because of the ongoing stiffening, also the wavelength of deformation continues to increase. This, in turn, promotes an additional change in the subsidence, which is now distributed over a broader area.

4.2. Effects of Thermal Blanketing by Sediments on the Transient Thermal Configuration of the Lithosphere

The transient effects of sediment blanketing on the resulting subsidence can be explained and quantified by properly considering the subsidence history of the plate as a function of heat and stress transfer within the joint system of the sedimentary blanket and the underlying crust and mantle lithosphere. With few exceptions (i.e., rock salt [*Lerche and O'Brien*, 1987]), the thermal conductivity of sedimentary rock is less than that of typical crystalline rocks that comprise the crust and the mantle lithosphere [*Arhens et al.*, 1995]. Therefore, the relatively slow deposition of sediments upon a background geothermal gradient produces an increase in lithospheric temperature by thermal blanketing from the sedimentary cover (Figure 8). The presence of the sedimentary pile on a thermally relaxing lithosphere mainly affects its rate of cooling, which is slower than for a case in which no sedimentation is considered. This is because thermal blanketing effectively counteracts rates of crustal heat transfer, thus reducing the amount of heat escaping at the surface. This is illustrated schematically in Figure 8, where temperature profiles are extracted from the 3-D model for the case considering (grey curves) and neglecting (black curves) sedimentation. Two time steps are illustrated. The first curves (dotted curves) refer to the beginning of stiffening at crustal level in Figure 4 b, that is, approximately at $t = 100$ Myr. The second curves are taken approximately synchronous to the

beginning of stress relaxation within the mantle, after 200 Myr of simulation time (dash-dotted curves). Even after 200 Myr after the starting of cooling, there is still a large amount of residual heat in a lithosphere consisting of a sedimentary pile of finite thermal conductivity (proportional to the grey areas in between the two curves). The presence of sediments results in a diffusive time scale which is more than double that of typical crustal rocks (constrained usually around 80 up to 100 Myr, e.g. [*McKenzie*, 1978]), thus having a strong effect on the overall subsidence pattern. A lithosphere cooling at slower rate strengthens slower than a lithosphere that is not blanketed by sediments; see Figure 4b. The mechanical effects of such configuration is to delay stress relaxation due to thermally activated creep in the mantle, thus leading to a slow thermal subsidence over geologic time as the one depicted in Figure 4a. Additionally, changes in the thermal field have a direct impact on the basic thermal and rheological properties of the lithosphere. Temperature variations cause variations in the rock density and therefore result in a different state of stresses acting on the plate. At the same time, due to the thermal dependence of mantle rock properties (namely, thermal conductivity and capacity), variations in the thermal configuration modify the ability of the lithosphere to contract thermally. The net result of all these interactions is again a slow though long-lasting thermal subsidence.

4.3. Effects of Mechanical Decoupling at Crust-Mantle Level

Observed deviations in the subsidence curves of intracontinental basins from their long-term linear trend have been often explained by changes in tectonic processes occurring at the adjacent plate margins [*Armitage and Allen*, 2010]. This has been demonstrated for some of the cratonic basins of North America, where periods of increased subsidence have been correlated to variations in intraplate stresses across the North Atlantic margin. However, for other intracontinental basins a tectonic explanation is not obvious [*Lambeck*, 1983; *Pawlak et al*., 2011; *Petersen et al*., 2010]. Our thermomechanical study supports the presence of a weak lower crust that could be therefore easily reactivated even under low-magnitude external forcing, thus plausibly initiating periods of increased subsidence as induced by superimposed far-field stresses. Furthermore, our results suggest that destabilization of the lower crust during basin subsidence may be followed by crust-mantle decoupling and by the onset of a tensile stress state in the lower crust (Figure 5a). Although no model developed short-term variations in subsidence, there is a propensity of the system to undergo supplementary crustal thinning by ductile flow, thus providing a complementary and intrinsic explanation to periods of increased subsidence.

4.4. Comparison With Natural Examples

In Figure 9 we compare 1-D subsidence curves as extracted from our 3-D model with reconstructed subsidence curves as published for intracontinental basins [*Xie and Heller*, 2009]. The comparison does not aim to provide a unique match with observations, which would have required taking into account geological and geodynamic details of each specific basin. It is rather intended to provide an alternative representation of the implications of the results derived from the study for real case settings. Therefore, while comparing the model results with observations, the reader should also consider the degree of simplification and lack of specific details of the modeling. Considering these aspects, modeled subsidence curves are found to be generally consistent with observations with respect to both the temporal behavior and the long-term subsidence trend. A correlation between model and observations is also found in terms of lithospheric configuration. Subsidence curves obtained from model realization based on an equilibrium thickness of 150 km provide a reasonable fit to reconstructed subsidence curves for relatively young intracontinental basins (e.g., North East German Basin and Paris basin). Curves obtained from model realizations based on a 200 km lithospheric thickness provide a better fit to those reconstructed for old, cratonic basins (e.g., Michigan basin). Model results show some deviations for two specific basins, that is, the Ordos and Illinois basins. Subsidence curves deviate from the observations mainly in relation to the initial stage of their subsidence history (first 100 Myr). The curve best matching the observations was found by imposing a slightly higher beta factor (1.6) than those considered in the manuscript for a 200 km lithosphere equilibrium thickness. Higher-magnitude thinning factors provided too steep subsidence curves. Previous studies suggested alternative and basin-specific processes to explain the observed anomalous initial subsidence in these two areas, related either to crustal metamorphism (Illinois basin [*Middleton*, 1980]) or to supracrustal deformation at the basin margins (Ordos basin [*Xie*, 2007]). If so, our predictions are still within the range of observations.

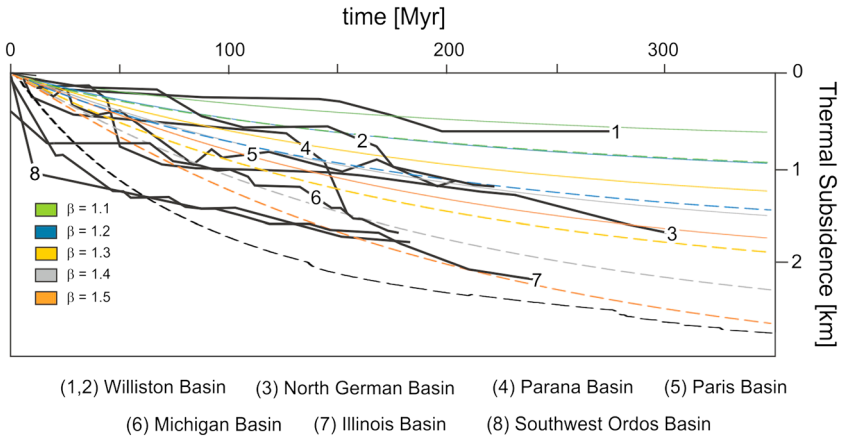

Figure 9. Comparison of modeled 1-D and reconstructed subsidence curves. Data are after *Xie and Heller* [2009]. Continuous curves refer to a 150 km equilibrium thickness, and dashed curves to a 200 km case. Different colors are here used to indicate different β factors imposed on the system.

4.5. The 2-D Versus 3-D Effects in Transient Thermal Models

Figure 10a shows the subsidence history of a stretched lithosphere initially 150 km thick, with (continuous curves) and without (dotted curves) sediments as obtained from a two-dimensional simulation. The respective model setup (i.e., boundary, initial, and model parameters) corresponds to the one described previously for the reference 3-D case. We obtained a two-dimensional solution by shrinking the model domain along the *y* plane to a single elemental volume, while maintaining the original extent along the other horizontal and vertical directions. Additionally, we imposed close boundary conditions (i.e., no flow boundary) across the *y* axis. Subsidence curves obtained for the corresponding 3-D are also shown by the dash-dotted curves. For all stretching factors, 2-D subsidence curves display trends with a very short in time initial subsidence phase of high rates followed by a long-lived subsidence characterized by lower rates, tailing off to an asymptotic value around approximately 150 Myr (Figure 10a). Within a two-dimensional approximation, lateral heat conduction is limited to a single dimension and the thermal blanketing effect by the sediments is therefore reduced. It follows that the retarding effect from the insulating sedimentary cover is reduced when compared to the 3-D case. Additionally, under similar loading conditions, a two-dimensional lithosphere bends more easily than a three-dimensional plate, and the former shows a longer flexural wavelength of deformation. Therefore, two-dimensional plate approximations tend to overemphasize the advective (vertical only) cooling component by sediment loading. The interplay of these two factors results in an increased strength within the upper crust and in a reduction of the initial subsidence in response to sediment loading. This explains

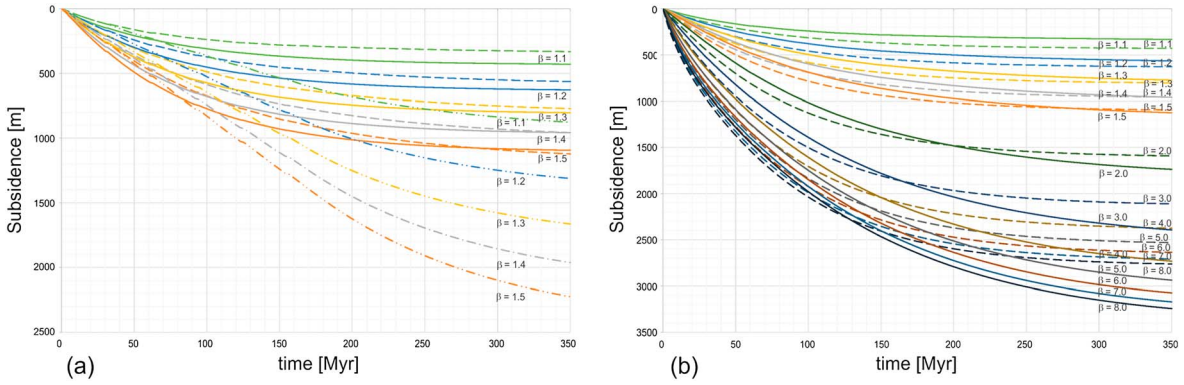

Figure 10. The 2-D versus 3-D effects in transient thermal models, and their influence on the long-term subsidence behavior. (a) Modeled subsidence curves obtained from a 2-D model realization with (continuous curves) and without (dashed curves) active sedimentation. Simulations are derived from a 150 km equilibrium thickness under β factors lower than 1.5; (b) modeled subsidence curves from a 2-D model approximation considering (continuous) and neglecting (dashed curves) the presence of sediments, 150 km equilibrium thickness but at higher β factors (up to 8). Subsidence curves as obtained from the 3-D model realization are also shown by the dash-dotted curves in both figures.

the lower subsidence rates obtained for the 2-D model realization accounting for active sedimentation in the early phase of the evolution of the system (approximately during the first 150 Myr) and the later exponential decay of subsidence that is dominantly controlled by the behavior of the cooling mantle.

For relatively low amounts of lithosphere thinning, the asymptotic lithospheric thickness of a lithosphere loaded by sediments is less than the thickness of a lithosphere in which no sediments have been deposited (Figure 10b). At higher stretching factors, that is, higher than 1.5, the two subsidence curves cross each other late in the evolution of the system, with an earlier in time crossing point for higher stretching factors (Figure 10b). The presence of a sedimentary cover, together with higher amounts of lithosphere thinning and related initial thermal destabilization, results in lithospheric configuration, which do not equilibrate within the 350 Myr of simulations considered. This is reflected by a prolonged subsidence, which does not tail off but gradually increases during the entire simulation, thus resembling subsidence curves of typical intracontinental settings. However, when compared to 3-D solutions, 2-D solutions require considerably higher stretching factors to produce comparable amounts of subsidence as for the 3-D case. If such strong lithosphere stretching were the case, the basin would also be affected by extensive brittle deformation in the form of basement faulting, a feature that is hardly observed in intracontinental basins. Likewise, stretching factors larger than 4 would cause the formation of decompressional melts, another feature rarely observed beneath intracontinental settings. The first-order differences found between 2-D and 3-D models raise some doubts whether two-dimensional approximations can correctly represent all thermomechanical interactions that occurred during the evolution of a basin for anything other than essentially two-dimensional phenomena. These differences hinge on 3-D thermomechanical feedback effects that cannot be properly addressed, if at all, by monodimensional or two-dimensional approaches.

5. Conclusions

Our results partly agree with previous studies in that we do conceive intracontinental basins as an extreme case of the rift-drift suite of basins forming under low stretching/thinning factors [*Armitage and Allen*, 2010]. However, to reconcile the first-order trends in their subsidence, our model does not require any specific condition for the initial lithospheric configuration, a rifting stage prolonged in time (if at all present) or a dynamic mantle component. We have demonstrated that the evolution of the lithosphere is sensitive to variations in the whole strength of the plate and that it is a function not only of the internal three-dimensional thermorheological configuration but of the loading history as well. By considering all these processes and their interdependency, it is possible to reconcile the basic characteristics observed in intracontinental settings.

A further and more generic implication from our study is that it also offers the possibility to assist retrodeformational studies and it helps in the quantification of the limitations commonly integrated in generic backstripping approaches [*Dressel et al.*, 2015].

While other processes (i.e., mantle convection or phase changes in the lower crust) might additionally affect the evolution of these systems, our study provides evidence that, to a first order, long-lived and slowly subsiding intracontinental basins can be explained as a consequence of 3-D thermal and mechanical feedback effects between sedimentation and thermal reequilibration at deeper crustal and mantle levels.

In the manuscript, we have started our discussion by focusing on the transient evolution of the strength of the lithosphere, but we have concluded with additional statements about the importance of considering 3-D thermal and mechanical effects when modeling the subsidence history of sedimentary basins. Our 3-D consideration entails that the detailed temporal evolution of the lithospheric strength, which controls the subsidence history, is strongly coupled to the temporal thermal configuration of the lithosphere and that it can only be addressed by a 3-D thermomechanical approach integrating laboratory-constrained mechanical data and transient lithospheric temperature configurations associated with the evolution of intracontinental basins.

Acknowledgments

The data for this paper, including the source code used to generate all results, are available upon request by contacting the corresponding author. The authors would like to thank John Armitage and an anonymous reviewer for helpfully pointing out where and how the paper could be improved and focused. Their suggestions and critic revisions helped improve the quality of the final publication.

References

Albert, R., R. Phillips, A. Dombard, and C. Brown (2006), A test of validity of yield envelopes with an elastoviscoplastic finite element model, *Geophys. J. Int.*, *140*, 399–409.

Arhens, T., C. Clauser, and E. Huenges (1995) Thermal conductivity of rocks and minerals, in *Rock Physics & Phase Relations: A Handbook of Physical Constants*, edited by T. J. Ahrens, AGU, Washington, D. C.

Armitage, J., and P. Allen (2010), Cratonic basins and the long-term subsidence history of continental interiors, *J. Geophys. Soc. Lond.*, *167*, 61–70.

Artemieva, I. (2006), Global 1° × 1° thermal model TC1 for the continental lithosphere: Implications for lithosphere secular evolution, *Tectonophysics*, *416*(1–4), 245–277.
Baird, D. J., J. H. Knapp, D. N. Steer, L. D. Brown, and K. D. Nelson (1995), Upper-mantle reflectivity beneath the Williston basin, phase-change Moho, and the origin of intracratonic basins, *Geology*, *23*(5), 431–434.
Berman, R., and T. Brown (1985), Heat capacity of minerals in the system Na_2O-K_2O-CaO-MgO-FeO-Fe_2O_3-Al_2O_3-SiO_2-TiO_2-H_2O-CO_2: Representation, estimation, and high temperature extrapolation, *Contrib. Mineral. Petrol.*, *89*, 168–183.
Braun, J., and R. Shaw (2001), A thin-plate model of Paleozoic deformation of the Australian lithosphere: Implications for understanding the dynamics of intracratonic deformation, *Geol. Soc. Spec. Publ.*, *184*, 165–193.
Braun, J., F. Deschamps, R. Delphine, and O. Dateuil (2013), Flexure of the lithosphere and the geodynamical evolution of non-cylindrical passive margins: Results from a numerical model incorporating variable elastic thickness, surface processes and 3D thermal subsidence, *Tectonophysics*, *604*, 72–82.
Buiter, S., B. Steinberger, S. Medvedev, and J. Tetreault (2012), Could the mantle have caused subsidence of the Congo basin?, *Tectonophysics*, *514–517*, 62–60.
Burgess, P. M., and M. Gurnis (1995), Mechanisms for the formation of cratonic stratigraphic sequences, *Earth Planet. Sci. Lett.*, *136*, 647–663.
Burgess, P. M., M. Gurnis, and L. Moresi (1997), Formation of sequences in the cratonic interior of North America by interaction between mantle, eustatic, and stratigraphic processes, *Geol. Soc. Am. Bull.*, *108*(12), 1,515–1,535.
Burov, E., and S. A. P. L. Cloetingh (1997), Erosion and rift dynamics: New thermomechanical aspects of post-rift evolution of extensional basins, *Earth Planet. Sci. Lett.*, *150*, 7–26.
Burov, E., and M. Diament (1995), The effective elastic thickness (Te) of continental lithosphere: What does it really mean?, *J. Geophys. Res.*, *100*, 3905–3927, doi:10.1029/94JB02770.
Coackley, B., and M. Gurnis (1995), Far-field tilting of Laurentia during the Ordovician and constraints on the evolution of a slab under an ancient continent, *J. Geophys. Res.*, *100*, 6,313–6,327, doi:10.1029/94JB02916.
Doin, M., and L. Fleitout (1996), Thermal evolution of the ocean lithosphere: An alternative view, *Earth Planet. Sci. Lett.*, *142*, 121–136.
Dressel, I., M. Scheck-Wenderoth, M. Cacace, B. Lewerenz, H.-J. Götze, and C. Reichert (2015), Reconstruction of the subsidence of the southwest African continental margin by backward modelling, *Mar. Petrol. Geol.*, *67*, 544–555.
Evans, B., J. Fredrich, and T. Wong (1990), The brittle-ductile transition in rocks: Recent experimental and theoretical progress, *Geophys. Monogr. Ser.*, *56*, 61–82.
Gac, S., R. Huismans, Y. Podlachikov, and J. I. Faleide (2012), On the origin of the ultradeep East Barents Sea basin, *J. Geophys. Res.*, *117*, B04401, doi:10.1029/2011JB008533.
Gilet, P., P. Richet, F. Guyot, and G. Fiquet (1991), High-temperature thermodynamic properties of Forsterite, *J. Geophys. Res.*, *96*, 11,805–11,816, doi:10.1029/91JB00680.
Gleason, G., and J. Tullis (1995), Flow law for dislocation creep of quartz and aggregates determines with the molten-salt cell, *Tectonophysics*, *247*, 1–23.
Gurnis, M. (1988), Large-scale mantle convection and the aggregation and dispersal of supercontinents, *Nature*, *344*, 695–699.
Hamdami, Y., J. C. Mareschal, and J. Arkani-Hamed (1994), Phase change and thermal subsidence of the Williston basin, *Geophys. J. Int.*, *116*, 585–597.
Hartley, R., and P. Allen (1994), Interior cratonic basins of Africa: Relation to continental break-up and role of mantle convection, *Basin Res.*, *6*, 95–113.
Heine, C., D. Müller, B. Steinberger, and T. Torvsik (2012), Subsidence in intracontinental basins due to dynamic topography, *Phys. Earth Planet. Inter.*, *171*, 252–264.
Hirth, G., and D. Kohlstedt (2003), Rheology of the upper mantle and the mantle wedge: A view from the experimentalists, *Geophys. Monogr.*, *138*, 83–105.
Holt, P., M. Allen, J. van Hunen, and H. Bjornseth (2010), Lithospheric cooling and thickening as a basin forming mechanism, *Tectonophysics*, *495*, 184–194.
Huang, J., and S. Zhong (2005), Sublithospheric small-scale convection and its implications for the residual topography at old ocean basins and the plate model, *J. Geophys. Res.*, *110*, B05404, doi:10.1029/2004JB003153.
Huismans, R., and C. Beaumont (2011), Depth-dependent extension, two-staged breakup and cratonic underplating at rifted margins, *Nature*, *472*, 74–78.
Kabongo, E. K., E. S. S. M. Ntabwoba, and F. Lucazeau (2011), A Proterozoic-rift origin for the structure and the evolution of the Congo basin, *Earth Planet. Sci. Lett.*, *204*, 240–250.
Kaminski, E., and C. Jaupart (2000), Lithosphere structure beneath the Phanerozoic intracratonic basins of North America, *Earth Planet. Sci. Lett.*, *178*, 139–149.
Karner, G. (1991), Sediment blanketing and flexural strength of extended continental lithosphere, *Basin Res.*, *3*, 177–185.
Kaus, B., Y. Podladchikov, and S. M. Schmalholz (2005), Effect of mineral phase transition on sedimentary basin subsidence and uplift, *Earth Planet. Sci. Lett.*, *233*, 213–228.
Klein, G., and A. Hsui (1987), Origin of intracratonic basins, *Geology*, *15*, 1,094–1,098.
Kusznir, N. (1982), Intraplate lithosphere strength and heat flow, *Nature*, *299*, 540–542.
Kusznir, N., and G. Karner (1985), Dependence of the flexural rigidity of the continental lithosphere on rheology and temperature, *Nature*, *316*, 138–142.
Lambeck, K. (1983), Structure and evolution of the intracratonic basins of central Australia, *Geophys. J. R. Astron. Soc.*, *74*, 843–886.
Lavier, L., and M. Steckler (1997), The effect of sedimentary cover on the flexural strength of continental lithosphere, *Nature*, *389*, 476–479.
Lerche, I., and O'Brien (1987), *Dynamic Geology of Salt and Related Structures*, Academic Press Inc., Ltd, London.
Littke, R., U. Bayer, D. Gajewski, and S. Nelskamp (Eds.) (2008), *Dynamics of Complex Intracontinental Basins—The Central European Basin System*, Springer, Berlin.
McKenzie, D. (1978), Some remarks on the development of sedimentary basins, *Earth Planet. Sci. Lett.*, *40*, 25–32.
McKenzie, D., and J. Priestley (2005), Thermal structure of oceanic and continental lithosphere, *Earth Planet. Sci. Lett.*, *233*, 337–349.
Middleton, M. F. (1980), A model for intracratonic basin formation, entailing deep crustal metamorphism, *Geophys. J. Int.*, *62*(1), 1–14.
Moresi, L., F. Dufour, and H.-B. Mühlhaus (2003), A Langragian integration point finite element method for large deformation model of viscoelastic geomaterials, *J. Comput. Phys.*, *184*(2), 476–497.
Nadai (1963), *Theory of Flow and Fracture of Solids*, vol. II (Revision of Plasticity), McGraw-Hill Book Company Inc, New York.
Nishida, A. (2010), Experience in developing an open source scalable software infrastructure in Japan, Computational Science and Its Applications ICCSA 2010, *Lect. Notes Comput. Sci.*, *6017*, 87–89.

Pawlak, A., D. Eaton, I. Baston, J.-M. Kendall, G. Helffrich, J. Wookey, and D. Snyder (2011), Crustal structure beneath Hudson Bay from ambient-noise tomography: Implications for basin formation, *Geophys. J. Int.*, *184*, 65–82.
Petersen, K. D., S. B. Nielsen, O. R. Clausen, R. Stephenson, and T. Gerya (2010), Small-scale mantle convection produces stratigraphic sequences in sedimentary basins, *Science*, *329*(5993), 827–830.
Ranalli, G. (1995), *Rheology of the Earth*, 2nd ed., Chapman & Hall, London.
Ranalli, G., and D. C. Murphy (1987), Rheological stratification of the lithosphere, *Tectonophysics*, *132*, 281–295.
Regenauer-Lieb, K., R. Weinberg, and G. Rosenbaum (2006), The effect of energy feedbacks on continental lithosphere, *Nature*, *446*, 67–70.
Rybacki, E., and G. Dresen (2000), Dislocation and diffusion creep of synthetic anorthite aggregates, *J. Geophys. Res.*, *105*, 26,017–26,036, doi:10.1029/2000JB900223.
Scheck, M., and U. Bayer (1999), Evolution of the Northeast German Basin—Inferences from a 3D structural model and subsidence analysis, *Tectonophysics*, *313*(1–2), 145–169.
Sleep, N. H., and L. L. Sloss (1980), The Michigan basin, in *Dynamics of Plate Interiors*, *Geodyn. Ser.*, vol. 1, edited by A. W. Bally et al., pp. 93–98, AGU.
Sloss, L. L. (1988), Introduction in sedimentary cover: North American Craton, *Geol. Soc. Am., Geol. North Am.*, *D-2*, 1–3.
Stein, C., and S. Stein (1992), A model for the global variation in oceanic depth and heat flow with lithospheric age, *Nature*, *359*, 123–129.
Tesauro, M., M. Kaban, and S. A. P. L. Cloetingh (2013), Global model for the lithospheric strength and effective elastic thickness, *Tectonophysics*, *602*, 78–86.
Xie, X. (2007), Sedimentary record of Mesozoic intracontinental deformation in the South Ordos basin, China, PhD thesis, Univ. of Wyoming.
Xie, X., and P. Heller (2009), Plate tectonics and basin subsidence history, *Geol. Soc. Am. Bull.*, *121*, 55–64.
Xu, Y., T. Shankland, S. Linhardt, D. Rubie, F. Langenhorst, and K. Klasinski (2004), Thermal diffusivity and conductivity of olivine, wadsleyite and ringwoodite to 20 GPa and 1373 K, *Earth Planet. Lett*, *143–144*, 312–336.
Zhang, Y. K. (1993), The thermal blanketing effect of sediments on the rate and amount of subsidence in sedimentary basins formed by extension, *Tectonophysics*, *218*, 297–308.
Zhong, S., M. Gurnis, and L. Moresi (1996), Free-surface formulation of mantle convection. I. Basic theory and application to plumes, *Geophys. J. Int.*, *127*, 708–718.